Quantitative X-ray wavefront measurements of Fresnel zone plate and K-B mirrors using phase retrieval

Xiaojing Huang[1]**, Nicolas Burdet**[2]**, Michael Wojcik**[3,4]**, Isaac Peterson**[5]**,
Graeme Morrison**[2]**, David Vine**[6]**, Daniel Legnini**[6]**, Ross Harder**[6]**,
Yong S. Chu**[1] **and Ian K. Robinson**[2,7]

[1]*National Synchrotron Light Source II, Brookhaven National Laboratory, Upton, NY 11973, USA*
[2]*London Centre for Nanotechnology, University College London, London, WC1H 0AH, UK*
[3]*Department of Physics, Illinois Institution of Technology, Chicago, IL 60616, USA*
[4]*Center for Nanoscale Materials, Argonne National Laboratory, Argonne, IL 60439, USA*
[5]*School of Physics, The University of Melbourne, Victoria 3010, Australia*
[6]*Advanced Photon Source, Argonne National Laboratory, Argonne, IL 60439, USA*
[7]*Research Complex at Harwell, Didcot, Oxfordshire OX11 0DE, UK*

i.robinson@ucl.ac.uk

Abstract: A scanning coherent diffraction imaging method was used to reconstruct the X-ray wavefronts produced by a Fresnel zone plate (FZP) and by Kirkpatrick-Baez (KB) focusing mirrors. The ptychographical measurement was conducted repeatedly by placing a lithographed test sample at different defocused planes. The wavefronts, recovered by phase-retrieval at well-separated planes, show good consistency with numerical propagation results, which provides a self-verification. The validity of the obtained FZP wavefront was further confirmed with theoretical predictions.

OCIS codes: (340.0340) X-ray optics; (100.5070) Phase retrieval; (110.3010) Image reconstruction techniques

References and links

1. C. Schroer, O. Kurapova, J. Patommel, P. Boye, J. Feldkamp, and B. Lengeler, "Hard x-ray nanoprobe based on refractive x-ray lenses," Applied Physics Letters **87**, 124,103 (2005).
2. K. Evans-Lutterodt, A. Stein, J. Ablett, N. Bozovic, A. Taylor, and D. Tennant, "Using Compound Kinoform Hard-X-Ray Lenses to Exceed the Critical Angle Limit," Physical Review Letters **99**(13), 134,801 (2007).
3. H. Mimura, S. Handa, T. Kimura, H. Yumoto, D. Yamakawa, H. Yokoyama, S. Matsuyama, K. Inagaki, K. Yamamura, Y. Sano, K. Tamasaku, Y. Nishino, M. Yabashi, T. Ishikawa, and K. Yamauchi, "Breaking the 10 nm barrier in hard-X-ray focusing," Nature Physics **6**, 122–125 (2010).
4. W. Chao, P. Fischer, T. Tyliszczak, S. Rekawa, E. Anderson, and P. Naulleau, "Real space soft x-ray imaging at 10 nm spatial resolution," Optics Express **20**(9), 9777–9783 (2012).
5. T. Chen, Y. Chen, C. Wang, I. Kempson, W. Lee, Y. Chu, Y. Hwu, and G. Margaritondo, "Full-field microimaging with 8 keV X-rays achieves a spatial resolutions better than 20 nm," Optics Express **19**(21), 19,919–19,924 (2011).
6. H. Yan, V. Rose, D. Shu, E. Lima, H. Kang, R. Conley, C. Liu, N. Jahedi, A. Macrander, G. Stephenson, M. Holt, Y. Chu, M. Lu, and J. Maser, "Two dimensional hard x-ray nanofocusing with crossed multilayer Laue lenses," Optics Express **19**(16), 15,069–15,076 (2011).
7. H. Quiney, A. Peele, Z. Cai, D. Paterson, and K. Nugent, "Diffractive imaging of highly focused X-ray fields," Nature Physics **2**, 101–104 (2006).
8. H. Yumoto, H. Mimura, S. Matsuyama, S. Handa, and Y. Sano, "At-wavelength figure metrology of hard x-ray focusing mirrors," Review of Scientific Instruments **77**, 063,712 (2006).

9. H. Mimura, H. Yumoto, S. Matsuyama, S. Handa, T. Kimura, Y. Sano, M. Yabashi, Y. Nishino, K. Tamasaku, T. Ishikawa, and K. Yamauchi, "Direct determination of the wave field of an x-ray nanobeam," Physics Review A **77**(1), 015,812 (2008).

10. M. Guizar-Sicairos and J. Fienup, "Measurement of coherent x-ray focused beams by phase retrieval with transverse translation diversity," Optics Express **17**(4), 2670–2685 (2009).

11. C. Kewish, P. Thibault, M. Dierolf, O. Bunk, A. Menzel, J. Vila-Comamala, K. Jefimovs, and F. Pfeiffer, "Ptychographic characterization of the wavefield in the focus of reflective hard X-ray optics," Ultramicroscopy **110**, 325–329 (2010).

12. C. Kewish, M. Guizar-Sicairos, C. Liu, J. Qian, B. Shi, C. Benson, A. Khounsary, J. Vila-Comamala, O. Bunk, J. Fienup, A. Macrander, and L. Assoufid, "Reconstruction of an astigmatic hard X-ray beam and alignment of K-B mirrors from ptychographic coherent diffraction data," Optics Express **18**, 23,420–23,427 (2010).

13. A. Schropp, P. Boye, J. M. Feldkamp, R. Hoppe, J. Patommel, D. Samberg, S. Stephan, K. Giewekemeyer, R. N. Wilke, T. Salditt, J. Gulden, A. P. Mancuso, I. A. Vartanyants, E. Weckert, S. Schder, M. Burghammer, , and C. G. Schroer, "Hard x-ray nanobeam characterization by coherent diffraction microscopy," Applied Physics Letters **96**, 091,102 (2010).

14. M. Guizar-Sicairos, K. Evans-Lutterodt, A. Isakovic, A. Stein, J. Warren, A. Sandy, S. Narayanan, and J. Fienup, "One-dimensional hard X-ray field retrieval using a moveable structure," Optics Express **18**(17), 18,374–18,382 (2010).

15. M. Guizar-Sicairos, S. Narayanan, A. Stein, M. Metzler, A. Sandy, J. Fienup, and K. Evans-Lutterodt, "Measurement of hard x-ray lens wavefront aberrations using phase retrieval," Applied Physics Letters **98**, 111,108 (2011).

16. F. Mastropietro, D. Carbone, A. Diaz, J. Eymery, A. Sentenac, T. H. Metzger, V. Chamard, and V. Favre-Nicolin, "Coherent x-ray wavefront reconstruction of a partially illuminated Fresnel zone plate," Optics Express **19**(20), 19,223–19,232 (2011).

17. A. Morgan, A. Martin, A. D'Alfonso, C. Putkunz, and L. Allen, "Direct exit-wave reconstruction from a single defocused image," Ultramicroscopy **111**, 1455–1460 (2011).

18. G. J. Williams, H. M. Quiney, B. B. Dhal, C. Q. Tran, K. A. Nugent, A. G. Peele, D. Paterson, and M. D. de Jonge, "Fresnel coherent diffractive imaging," Physical Review Letters **97**(2), 025,506 (2006).

19. B. Abbey, K. Nugent, G. Williams, J. Clark, A. Peele, M. Pfeifer, M. D. Jonge, and I. McNulty, "Keyhole coherent diffractive imaging," Nature Physics **4**, 394–398 (2008).

20. J. Rodenburg, A. Hurst, A. Cullis, B. Dobson, F. Pfeiffer, O. Bunk, C. David, K. Jefimovs, and I. Johnson, "Hard-X-Ray Lensless Imaging of Extended Objects," Physical Review Letters **98**, 034,801 (2007).

21. P. Thibault, M. Dierolf, A. Menzel, O. Bunk, C. David, and F. Pfeiffer, "High-resolution scanning x-ray diffraction microscopy," Science **321**, 379–382 (2008).

22. P. Thibault, M. Dierolf, O. Bunk, A. Menzel, and F. Pfeiffer, "Probe retrieval in ptychographic coherent diffractive imaging," Ultramicroscopy **109**, 338–343 (2009).

23. A. Maiden and J. Rodenburg, "An improved ptychographical phase retrieval algorithm for diffractive imaging," Ultramicroscopy **109**, 1256–1262 (2009).

24. M. Dierolf, A. Menzel, P. Thibault, P. Schneider, C. Kewish, R. Wepf, O. Bunk, and F. Pfeiffer, "Ptychographic X-ray computed tomography at the nanoscale," Nature **467**, 436–440 (2010).

25. K. Giewekemeyer, M. Beckers, T. Gorniak, M. Grunze, T. Salditt, and A. Rosenhahn, "Ptychographic coherent x-ray diffractive imaging in the water window," Optics Express **19**(2), 1037–1050 (2011).

26. Y. Takahashi, A. Suzuki, N. Zettsu, Y. Kohmura, Y. Senba, H. Ohashi, K. Yamauchi, and T. Ishikawa, "Coherent x-ray wavefront reconstruction of a partially illuminated Fresnel zone plate," Physics Review B **83**(21), 214,109 (2011).

27. P. Godard, G. Carbone, M. Allain, F. Mastropietro, G. Chen, L. Capello, A. Diaz, T. Metzger, J. Stangl, and V. Chamard, "Three-dimensional high-resolution quantitative microscopy of extended crystals," Nature Communications **2**, 568 (2011).

28. *APS Science 2011* (Argonne National Laboratory, 2012).

29. K. Nugent, "Coherent methods in the x-ray sciences," Advanced Physics **59**, 1–99 (2010).

30. T. Kupp, B. Blank, A. Deyhim, C. Benson, I. Robinson, and P. Fuoss, "Development of a double crystal monochromator," AIP Conference Proceedings **CP705**, 651–654 (2004).

31. ZonePlates Ltd, 8 South Way, Claverings Industrial Estate, London N9 OAB, UK., URL http://www.zoneplates.com.

32. M. Wojcik, V. Joshi, A. Sumant, R. Divan, L. Ocola, M. Lu, and D. Mancini, "Nanofabrication of x-ray zone plates using ultrananocrystalline diamond molds and electroforming," Journal of Vacuum Science & Technology B **28**(6), C6P30–C6P35 (2010).

33. J. Butler and A. Sumant, "The CVD of Nanodiamond Materials," Chemical Vapor Deposition **14**, 145–160 (2008).

34. J. W. Goodman, *Introduction to Fourier Optics*, 3rd ed. (Roberts and Company, Englewood, 2004).

35. P. Eng, M. Newvile, M. Rivers, and S. Sutton, "Dynamicaly figured Kirkpatrick Baez X-ray micro-focusing optic," SPIE **3449**, 145–156 (1998).

1. Introduction

Recent developments in optics fabrication techniques have provided focused X-ray beam sizes in tens-of-nanometer size range, by a variety of formations: compound refractive lens [1], Kinoform lens [2], Kirkpatrick-Baez mirrors [3], Fresnel zone plate [4, 5] and multilayer Laue lens [6]. Characterization of the resulting X-ray focused beam wavefront is of fundamental importance for evaluating the fabrication and alignment qualities of focusing optical elements [7, 8, 9, 10, 11, 12, 13, 14, 15, 16, 17].

Quantitative wavefront measurement is also extremely valuable for the purpose of reliably obtaining artifact-free images with arbitrary sizes. In lens-less coherent diffraction imaging (CDI) methods specifically, the image obtained through phase retrieval is the product of the object and the illumination function. If the incident X-ray wavefront is not sufficiently uniform over the sample, the beam structure will be present mixed in with the image of the object. Phase-retrieval based approaches for wavefront measurement can reconstruct the complex wavefront using the far-field diffraction intensity of the beam itself with a priori knowledge of the optics aperture [7]. The accurately determined wavefront function can then serve as a scannable probe [18, 19], and thus release the limitation on field of view to imaging samples with arbitrary sizes. Alternatively, introducing translational diversity into coherent diffraction imaging measurement provides extra constraints arising from overlapping, redundantly illuminated sample sections. This general ptychographic approach can remove requirements on the maximum sample dimensions [20]. This redundancy also enables the factorisation of the illuminating beam while recovering the object image simultaneously [21, 22, 23, 24, 25, 26, 27]. Because they also characterize the incident beam wavefront, these generalized ptychography approaches have been approved to be very robust for handling noise and eliminating ambiguities. Widely used algorithms are based on the Difference Map [21] and the extended Ptychographic Iterative Engine (ePIE) [23].

In this work, we conducted X-ray wavefront measurements on the focused beams produced by FZP and KB mirrors by scanning a test pattern transversely across the beam. To verify the accuracy of the recovered illumination function, the measurement was performed at 3 defocused planes. Excellent agreement between the recovered wavefronts at each plane, which should be related by Fresnel propagation, was confirmed by numerical propagation. This approach verifies experimentally that the retrieved complex probe descriptions contain the correct convergent or divergent information within their phase structure.

2. Experimental setup

Fig. 1(a) illustrates the experimental setup at the 34-ID-C beamline of Advanced Photon Source, Argonne National Laboratory. The coherence and illumination-defining slits are 54.5 m (Z_v) away from the center of the Undulator A. The vertical X-ray beam source size σ_v is 26 μm [28]. To increase the horizontal coherence length, a 100 μm wide beam was selected horizontally by slits in front of a mirror, located 27.5 m in front of the coherence-defining entrance slits. With this setup, the half width at half maximum (HWHM) transverse coherence lengths can be estimated using $2\lambda Z\sqrt{\ln 2}/(\pi\sigma)$ [29] to be 20×154 μm (horizontal $\times$ vertical). The slit gaps were adjusted to select the coherent part of the incident X-ray beam.

An X-ray energy of 9 keV ($\lambda = 0.138$ nm) was selected by the beamline Si(111) double crystal monochromator [30], which provides sufficient longitudinal (temporal) coherence for this experiment.

A customized test pattern (shown in Fig. 1 (b)) was designed by us and fabricated by Zone-Plates Ltd [31] using electron beam lithography and Reactive Ion Etching (RIE). The pattern was prepared in 1.5 μm thick tungsten film evaporated on to a 100 nm thick silicon nitride window, to provide about 70% intensity transmission and about 0.8 π phase shift to a 9 keV
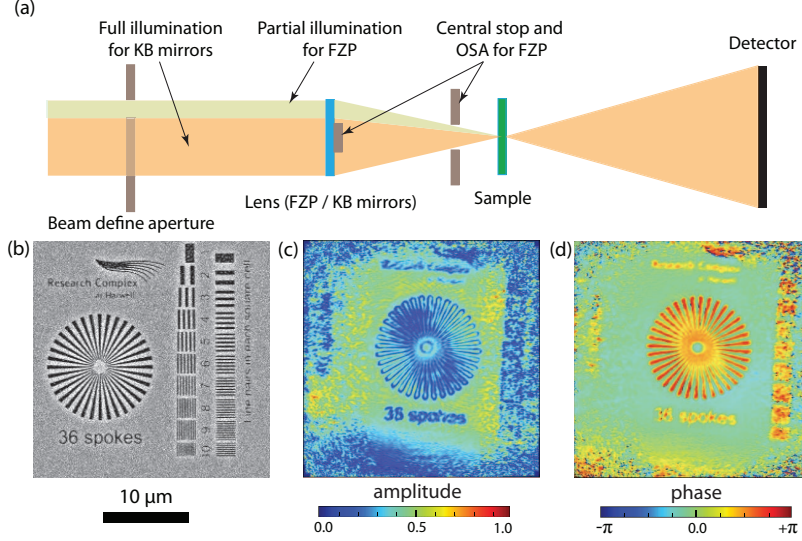
Fig. 1. (a) Sketch of the experimental setup. (b) SEM image of the test pattern. (c) A typical reconstructed magnitude image. (d) A typical reconstructed phase image.

X-ray beam. The test pattern was illuminated by an X-ray beam focused by the optics under investigation: the FZP or the KB mirror system. The ptychographical measurement was performed by translating the sample in the transverse plane. The sample was scanned using nPoint NPXY100Z25A piezo stage, which was mounted on the top of a set of XYZ step-motors for larger range movements. The scanning trajectory follows concentric circles, with $5n$ points on the nth ring and a radius increment of 0.5 μm for FZP and 0.75 μm for KB mirrors.

A Princeton Instrument PI-MTE 1300B charge-coupling device (CCD) with 20×20 μm pixel size was placed 2.31 m downstream from the test sample. The detector region-of-interest (ROI) was set to 400×400 pixels for FZP and 280×280 pixels for KB mirror measurements, which gives the real-space pixel size of 40 nm and 56.8 nm, respectively.

3. Focused wavefront from the Fresnel zone plate

The FZP we used in this work contains 2 μm thick alternating gold and diamond zones [32]. The diameter is 180 μm with 80 nm outer-most zone width and a 30 μm diameter central stop. With 9 keV X-rays, the first-order focus length is 104.5 mm. It was fabricated using ultra-nanocrystalline diamond (UNCD) as the dielectric mold material into which Au is electroplated. UNCD is a chemical vapor deposition (CVD) diamond composed of 2-5 nm grains of diamond bonded together with graphitic type bonds [33]. A 2-μm-thick layer of UNCD was prepared on 40 nm of tungsten and 1 μm of Si_3N_4 supported by a Si substrate. These layers were released to form a membrane by back etching the Si substrate. The sample was then coated with hydrogen silsesquioxane (HSQ) acting as the resist material and exposed using a 100 keV e-beam lithography system. After development, UNCD was etched with oxygen plasma designed for high anisotropy and selectivity. The resulting mold was filled by electroplating gold using tungsten as the conductive base. The HSQ was removed and the resulting FZP consists of alternating Au and UNCD zones.

The zone plate was mounted 286 mm downstream of the beam defining slits, about 104 mm before the sample. Considering the transverse coherence lengths at the zone plate plane are not sufficient to cover its entire 180 μm diameter, the beam-defining slits were set to 20×100 μm
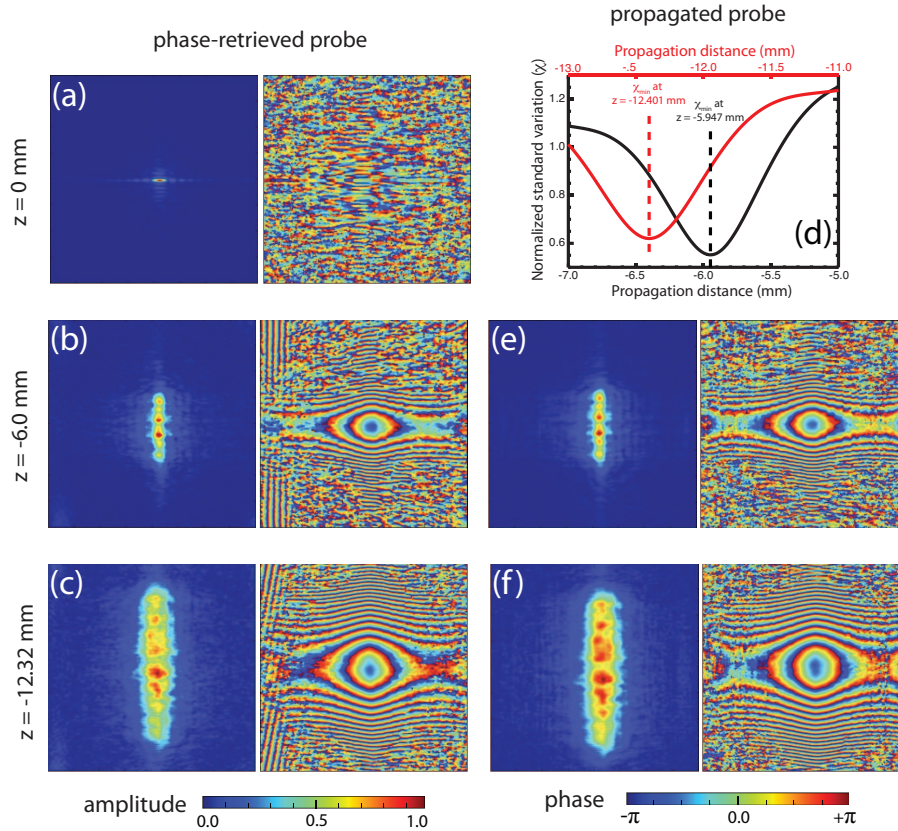
Fig. 2. (a)(b)(c) The phase-retrieved probe for FZP with the test sample placed at 0.0 mm, -6.0 mm and -12.32 mm. (d)(e) The simulated probes propagated from (c). (f) The propagation distances were determined by minimizing the standard variation between propagated and phase-retrieved probes.

(horizontal × vertical) to select the coherent beam and produce a partial illumination of the FZP [16]. The slits were offset by 35 μm in the horizontal direction to avoid the central stop and produce the separation between the first order focussed beam and the zeroth order direction beam, which is blocked by a 40 μm diameter order sorting aperture (OSA) mounted 85 mm away from the FZP, 19 mm in front of the sample.

A concentric scan pattern, chosen for the purpose of eliminating grid artifacts [22], with 10×10 μm scan range and 0.5 μm radius increment, generates 323 frames of far field diffraction patterns for one ptychographical measurement. A reconstruction strategy as described by Thibault [21] was used to recover the images of the sample and the illumination probe. A typical reconstructed test sample image is shown in Fig. 1 (c) and (d). The first measurement was performed at a plane denoted as $z = 0$ mm. The same ptychographical measurement was repeated at 2 different defocus positions with z step-motor readings of $z = -6.0$ mm and $z = -12.32$ mm, respectively, while the positive z points the downstream direction of the X-ray beam. The recovered probe wavefronts are shown in Fig. 2 (a), (b) and (c). Considering that these wavefronts at different planes are related by free space Fresnel propagation [34], to confirm the validity of the phase-retrieved X-ray wavefronts, we started with the recovered probe at $z = 0$ mm plane, and propagated it backwards to the other two planes. A half-pixel size sampling interval was used

in the Fresnel propagation calculation, upon Discrete Fourier Transformation in an array of 800 × 800. To compensate the positioning inaccuracy introduced by the z step-motor, the propagation distances were selected by minimizing the standard variation between the propagated and phase-retrieved probes (shown in Fig. 2 (d)). The best-matching propagation distances for the other two measurements located at $z = -5.947 \pm 0.241$ mm and $z = -12.401 \pm 0.172$ mm, respectively. The discrepancy between the measured and best-fit sample plane distances exceeds the expected errors with the motor stage, which is most likely attributed to a combination of phase-retrieval error and numerical propagation uncertainty. The probe images obtained from numerical propagations (shown in Fig. 2(e)(f)) show good consistency to the phase-retrieved probes (shown in Fig. 2(b)(c)). Fig. 3 shows a quantitative comparison between phase-retrieved and propagated probes. Both the amplitude and phase match very well, which confirms that the recovered phases are correct.
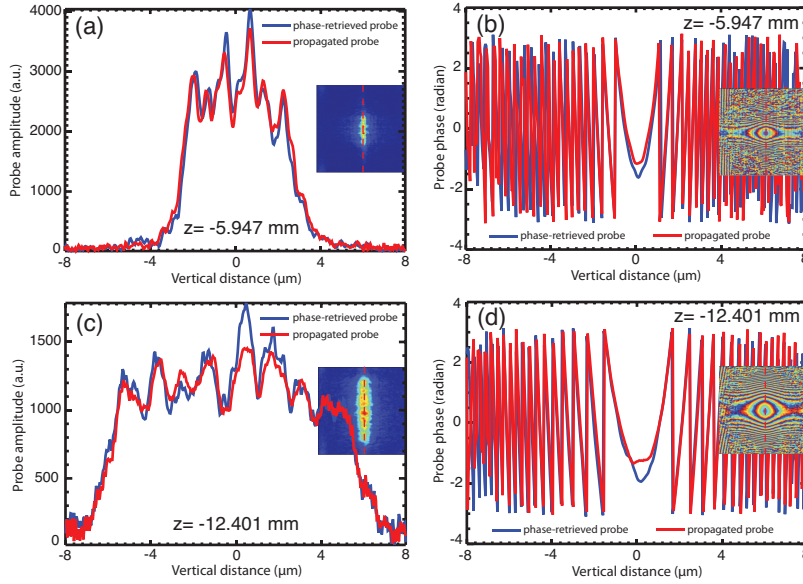

Fig. 3. Quantitate comparison of phase-retrieved and numerically propagated probes along the central vertical lines: the amplitude (a) and phase (b) plots at $z = -5.947$ mm, the amplitude (c) and phase (d) plots at $z = -12.401$ mm.

The fully recovered complex wavefront allows one to propagate it to any other plane in both the forward and backward directions. We propagated the reconstructed probe at $z = 0$ mm with 10 μm propagation step size in 20 mm range. Fig. 4 (a) and (b) shows horizontally-integrated and vertically-integrated intensities of the propagation profiles. In order to precisely locate the focal planes, a finer propagation with 1 μm step size was perform in the neighborhood of $z = 0$ mm. The propagation was repeated with 10 individually phase-retrieved probes obtained from different random starts, and the vertical and horizontal waist planes with narrowest peaks were selected from each propagation. Averaging these propagation results reveals that the vertical and horizontal focuses locate at 65 μm and 322 μm upstream of $z = 0$ mm plane, and the separation of those 2 focal planes is 257 ± 68 μm. The horizontal and vertical focus sizes are 730 nm and 168 nm, respectively, as shown in Fig. 6 (a) and (b).

Considering the focused wavefront as a demagnified image of the light source, if the horizontal and vertical X-ray sources located at different distances from the FZP, it can cause separated foci in the different directions. In the 34-ID-C beamline, the undulator center served as the
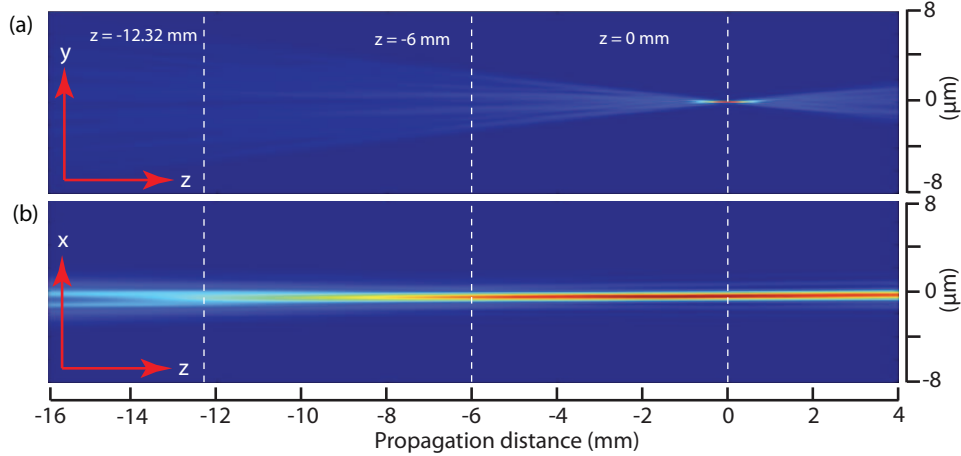
Fig. 4. Propagation of the phase-retrieved probe obtained at $z = 0.0$ mm: (a) intensity along the vertical direction, horizontally integrated, (b) intensity along the horizontal direction, vertically integrated.

vertical source, and a horizontal secondary source of 100 μm was set by a white-beam slit at the beamline mirror location. A simple calculation using the lens law gives that the separation of horizontal and vertical focal planes should be 195 μm, which agrees with the experimental result of 257$\pm$68 μm within measurement uncertainty. This 62 μm discrepancy may be due to fabrication or alignment issues with the FZP (see below) or due to incorrect functioning of the secondary source, which will be investigated further.

The additional 62 μm separation between the vertical and horizontal foci may suggest that the FZP was not perfectly perpendicular to the incident X-ray beam. The misalignment angle can be estimated by $\Delta = f(1 - \cos\theta) \approx f\sin^2\theta/2$, where Δ is the focus separation, f is the focal length, and θ is the misalignment angle between the FZP norm direction and the incident X-ray beam direction. Because the 20$\times$100 μm illumination-defining slits were offset horizontally, this setup is not sensitive to horizontal misalignment angle. The observed focus separation was thus mainly caused by vertical misalignment angle. With additional 62 μm separation and 104.5 mm focal length, the vertical misalignment angle is about 2 degree. When setting up the FZP, we used a diode laser to duplicate the X-ray beam path, and accommodated the FZP orientation to overlap the reflected laser beam from the FZP surrounding frame with the incident laser beam. The reflected laser dot was diverged to about 5 mm when a screen was placed about 0.5 m away from the FZP, which gave an alignment uncertainty of about 0.6 degree. Another error source arises from the norm direction difference between the FZP and its surrounding frame caused by stress related ripples. These uncertainties may accumulate to give 2 degree angular misalignment.

The focusing performance of the FZP can be simulated using its fabrication and experimental setup parameters[16]. A perfect FZP with 80 nm outer-most zone width and 180 μm diameter was simulated using alternating gold and diamond zone with 2 μm thickness. A uniform plane wave illumination was assumed in front of the 20 $\times$ 100 μm (horizontal $\times$ vertical) beam-defining slits. It then propagated 286 mm to the FZP. The wavefront modified by the FZP continued to propagate by 85 mm, where the outer wavefront was masked out by a 30 μm diameter OSA. The wavefront propagated by another 19.5 mm to reach the focal plane. Notice that the phase-retrieved wavefront presents alternatively dim horizontal fringes, especially in the top-half plane as shown in Fig. 5 (a). The missing fringes and asymmetry in the probe
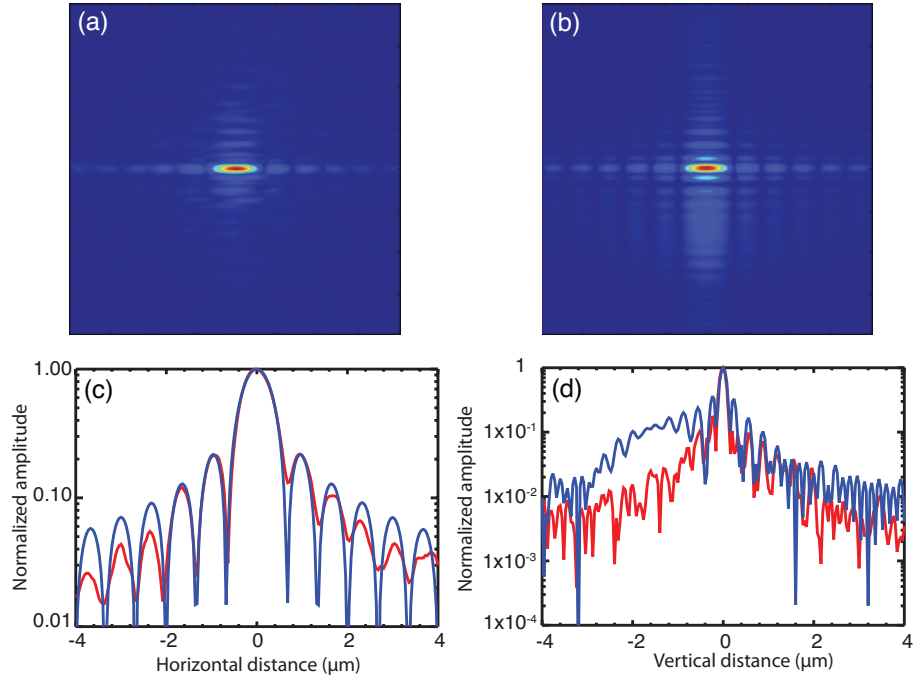
Fig. 5. Comparison between the recovered wavefront (a) through phase-retrieval and the simulated wavefront of FZP focused beam (b). The central 8×8 μm area is shown. (c) The amplitude plotted along the horizontal central line. (d) The amplitude plotted along the vertical central line.
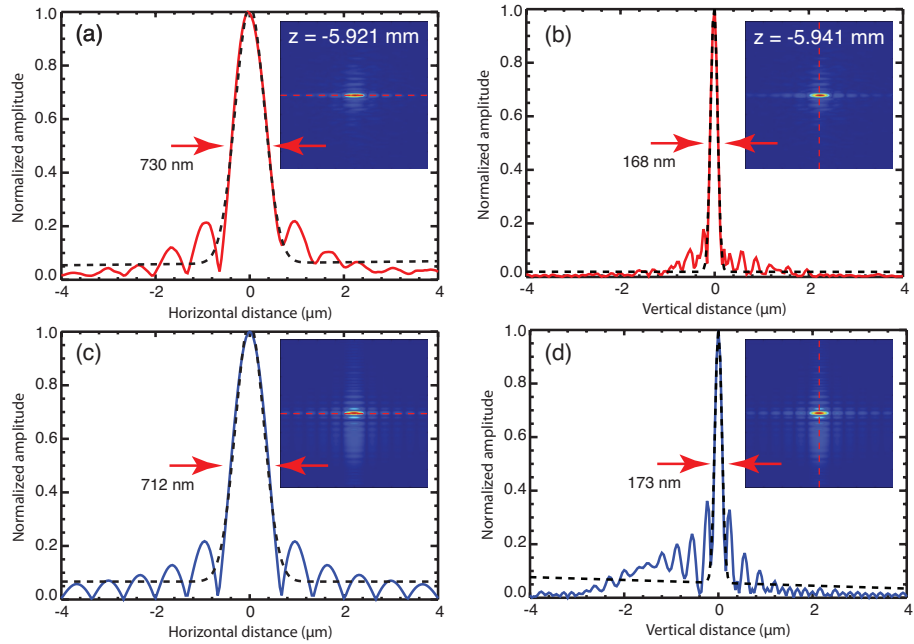

Fig. 6. Estimation of focal sizes of the phase-retrieved wavefront (a)(b) and the simulated wavefront (c)(d).

implies a phase-ramp might be introduced by FZP imperfection. Such a phase ramp with 2π extent and 90 μm width was simulated into the FZP, and the simulated focus is shown in Fig. 5 (b). The major features are consistent with the phase-retrieved the probe (Fig. 5 (c) (d)). The horizontal and vertical focus sizes of the simulated wavefront are 712 nm and 173 nm, respectively (Fig. 6 (c) (d)), which agree very well with the focus sizes of the recovered probe, 730 nm×168 nm (Fig. 6 (a) (b)), considering that the reconstruction pixel resolution is 40 nm.

4. Focused wavefront from Kirkpatrick Baez mirrors
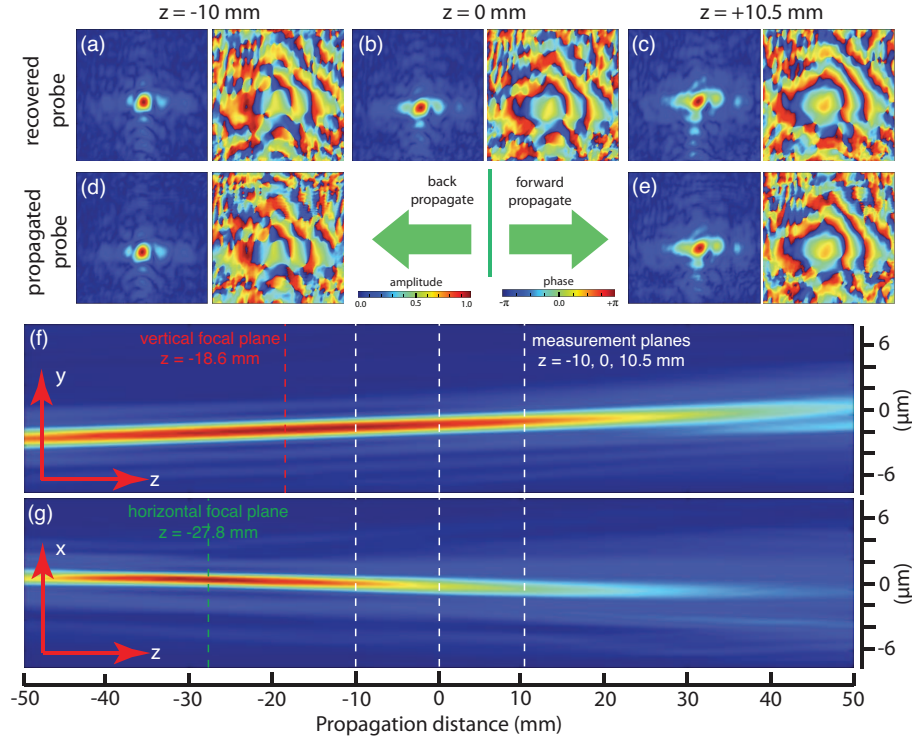
Fig. 7. (a)(b)(c) The reconstructed probe of the KB mirrors with the sample placed at -10 mm, 0.0 mm and 10.5 mm. (d)(e) The simulated probes propagated from (b). (f)(g) The integrated vertical and horizontal amplitude through focus.

Ptychographical measurements were conducted with Kirkpatrick-Baez (KB) mirrors using the same concept. The experimental setup was identical to FZP experiment, except for no OSA inserted in the optics path. The bendable KB mirrors [35] were coated with 50 platinum on top of a 10 nm chrome under-layer. The center of the 100 mm long vertical focusing mirror was placed 220 mm in front of the sample plane. The 100 mm long horizontal focusing mirror was 120 mm in front of the sample plane. The incident angle was set to 3 μrad for both of them. The illumination-define slits were 120 mm upstream of the entrance side of the vertical focusing mirror, and the entrance slit opening was set to 20×20 μm. The same lithographed test object was used to measure the wavefront in the sample plane.

The scan trajectory covered 10×10 μm range with 0.75 μm step size for radius increment, which created 141 frames of diffraction patterns for each complete ptychographcial scan. The measurement was repeated at $z = -10.0$ mm, 0.0 mm and $+10.5$ mm. The phase-retrieved X-ray beam wavefronts are shown in Fig. 7 (a)(b)(c). The recovered probe at $z = 0.0$ mm

was numerically propagated to -10 mm and $+10.5$ mm planes. The propagated wavefronts are shown in Fig. 7 (d) and (e), which are in good agreement with the reconstructed probes. Although the lack of metrology measurement of KB mirrors prevents numerical simulation of their focusing behavior, the consistency between recovered and propagated probes provides satisfactory confidence for the measurement.

The phase-retrieved probe was propagated in a range of 100 mm with 100 μm propagation step size. The horizontally and vertically integrated intensities at different planes are shown in Fig. 7 (f) and (g). We found that the vertical focal plane was located at $z = -18.6$ mm, and the horizontal focal plane was at $z = -27.8$ mm. The horizontal and vertical focal sizes were estimated to be 0.935 μm and 1.321 μm, respectively, as shown in Fig. 8. These numbers are systematically smaller than the 1.6 μm size routine obtained by scanning a 100 μm tungsten wire through the focus during the alignment of the KB benders. This discrepancy is understood to come from partial penetration of the X-ray beam into the edge of the wire.
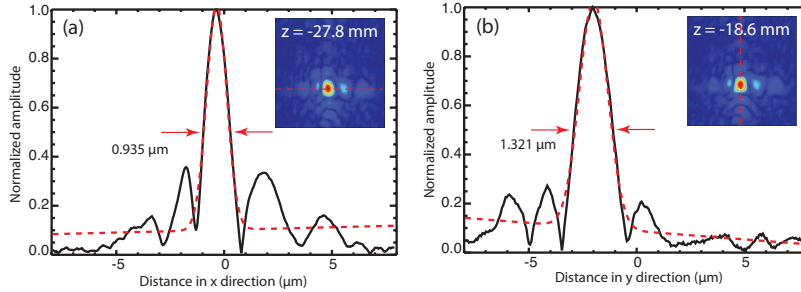

Fig. 8. Horizontal (a) and vertical (b) focal sizes of the Kirkpatrick-Baez (KB) mirror system at their corresponding focal planes.

5. Conclusion

Ptychographical measurements of the focused X-ray beam produced by Fresnel zone plate and KB mirrors were conducted with a test sample at various defocused planes. Phase-retrieved wavefronts at the different planes show good agreement with numerical propagations starting from the smallest recovered probe. For the FZP, the recovered focus is also consistent with a numerically simulated wave function of its focal plane. Both measurements confirm that the ptychographical approach is capable of providing robust and reliable X-ray probe functions. The repeated measurements at different defocused planes produce a convincing self-verification of the analytical method recovering the correct probe phase information, which is important in describing the focus.